Monte Carlo simulations of dense gas flow and heat transfer in micro- and nano-channels

WANG Moran & LI Zhixin

Department of Engineering Mechanics, Tsinghua University, Beijing 100084, China
Correspondence should be addressed to Li Zhixin (email: lizhx@tsinghua.edu.cn)
Received April 18, 2004

Abstract The dense gas flow and heat transfer in micro- and nano-channels was simulated using the Enskog simulation Monte Carlo (ESMC) method. The results were compared with those from the direct simulation Monte Carlo (DSMC) method and from the consistent Boltzmann algorithm (CBA). The dense gas flow and heat transfer characteristics were thus analyzed. The results showed that when the gas density was large enough, the finite gas density effect on the flow and heat transfer cannot be ignored, which decreased the skin friction coefficient and changed the heat transfer characteristics on the channel wall surfaces.

Keywords: dense gas flows, micro- and nano-channels, Monte Carlo simulation, Enskog equation.

DOI: 10.1360/03ye0511

The flow and heat transfer in micro/nano electro-mechanical-systems (MEMS/NEMS) is an important theoretical problem, which drives or restricts the further development of MEMS/NEMS. Now this kind of studies are of hot activity[1,2]. Due to the small characteristic length, the gas in micro- and nano-channels shows different features from the one in flow and heat transfer at macroscale. Generally, the mean free path of gas, even under common temperature and pressure, could be comparable to the characteristic length of the microscale channel, which results in a large Knudsen number, and therefore the rarefied gas effect could be remarkable on the transport process. In fact, the velocity slip and temperature jump on the surface have been validated both in theory and in experiments for micro gas flows[3].

Tsien[4] ever presented a detail analysis on similarity of rarefied gas flows in 1946. In recent years, a few researchers have introduced this similarity into the investigation of micro gas flows[5−7]. It was pointed that the micro gas flow could be similar to the rarefied gas flow as long as the perfect gas assumption was satisfied[7]. This result made much convenience for the studies on the micro gas flow. A lot of theories and modeling methods for the rarefied gas have been successfully applied in micro flow investigations[3,7]. However, in MEMS/NEMS another case could be met where the gas is not only in high Knudsen number but also in high density (pressure)[8]. In such cases, the

continuum assumption breaks down and the continuum-based theory cannot provide correct predictions; also the perfect gas assumption fails down, and the present rarefied gas theory and modeling methods are invaluable. Alexander et al.[9] proposed a consistent Boltzmann algorithm (CBA), and tried to expand the rarefied-and-perfect-gas-assumption based direct simulation Monte Carlo (DSMC)[10] method to dense gas and even liquid, by introducing an additional displacement after the molecular collisions. This modification replaced the equation of state (EOS) for perfect gas by the van der Waals equation. This method has been applied successfully in modeling of nuclear flow[11], gas- liquid interface characteristics[12], and micro and nanoscale non-ideal gas flow[13]. However, it was also noticed that the additional displacement changed not only the EOS but also the gas transport characteristics. As a result, when the gas molecular volume to the whole volume ratio was high, the gas transport would depart greatly and make the predictions failure[14−16].

Enskog modified the Boltzmann-based hard sphere model in 1922, and presented the famous Enskog equation for the finite gas density effect[17]:

$$\left(\frac{\partial}{\partial t}+\boldsymbol{v}\cdot\frac{\partial}{\partial \boldsymbol{r}}\right)f(\boldsymbol{r},\boldsymbol{v},t)=\sigma^2\int \mathrm{d}\boldsymbol{v}_1\int \mathrm{d}\hat{\boldsymbol{\sigma}}\Theta(\hat{\boldsymbol{\sigma}}\cdot\boldsymbol{g})(\hat{\boldsymbol{\sigma}}\cdot\boldsymbol{g})$$
$$\times[\chi(\boldsymbol{r},\boldsymbol{r}-\boldsymbol{\sigma})f(\boldsymbol{r},\boldsymbol{v}',t)$$
$$\times f(\boldsymbol{r}-\boldsymbol{\sigma},\boldsymbol{v}_1',t)-\chi(\boldsymbol{r},\boldsymbol{r}+\boldsymbol{\sigma})$$
$$\times f(\boldsymbol{r},\boldsymbol{v},t)f(\boldsymbol{r}+\boldsymbol{\sigma},\boldsymbol{v}_1,t)]. \tag{1}$$

where $\Theta(x)$ is the Heaviside function, $\boldsymbol{r}$ is the coordinate vector, $\boldsymbol{\sigma}=\sigma\hat{\boldsymbol{\sigma}}$, σ is the molecular diameter, $\boldsymbol{g}\equiv\boldsymbol{v}-\boldsymbol{v}_1$, $\boldsymbol{v}'=\boldsymbol{v}-(\hat{\boldsymbol{\sigma}}\cdot\boldsymbol{g})\hat{\boldsymbol{\sigma}}$, and $\boldsymbol{v}_1'=\boldsymbol{v}_1+(\hat{\boldsymbol{\sigma}}\cdot\boldsymbol{g})\hat{\boldsymbol{\sigma}}$.

Unfortunately, the Enskog equation is more complex and harder to solve than the Boltzmann equation. Recently, simplified kinetic models that keep the essential features of the Enskog equation have been proposed[18]. As in the case of the Boltzmann equation, a different approach consists of solving the Enskog equation by means of a numerical Monte Carlo algorithm in the same spirit as the DSMC method of solving the Boltzmann equation[19]. Montanero and Santos[20] presented an Enskog simulation Monte Carlo (ESMC) method similar as Nanbu's DSMC. Subsequently, they[21] and Frezzotti[22] indicated respectively that a new ESMC method similar as Bird's DSMC had better computational efficiency and did better in momentum and energy conservations. The previous research was creative and fundamental, however, the aspects on the dense gas simulation was still qualitative. This paper developed the latter ESMC method, and used this method for modeling and analyzing the flow and heat transfer characteristics of high-Knudsen-number and high-density gas flow in micro- and nano-channels.

1 Numerical method

1.1 Enskog simulation Monte Carlo (ESMC)

The Enskog simulation Monte Carlo (ESMC) method used in this paper was first

presented by Montanero and Santos[20,21]. Similar as the DSMC method, it solves the dynamic equations for gas flow by at least thousands of simulated molecules. Each simulated molecule represents a large number of real molecules. The molecules motion and their collisions are uncoupling if the grid size is much less than the gas mean free path ($\Delta L \ll \lambda$) and the computational time step is smaller than the physical collision time ($\Delta t < \tau$). The difference between ESMC and DSMC lies on the collision implements. In ESMC the collision of particles $i = 1, \cdots, N$ can be described as follows.

(i) For the particle *i*, get a random direction $\hat{\boldsymbol{\sigma}}_i$;

(ii) select collision pair in the direction $\boldsymbol{r}_i + \sigma\hat{\boldsymbol{\sigma}}_i$ from nearby particles. If there is no particles in the local cell, select one from the neighboring cells;

(iii) if the probability of collision between particle *i* and particle *j* is larger than $\chi(\boldsymbol{r}_i, \boldsymbol{r}_i + \sigma\hat{\boldsymbol{\sigma}}_i) \cdot \omega_{\mathrm{B}}$, the collision is accepted, where ω_{B} is the binary collision probability based on Boltzmann equation;

(iv) if the collision is accepted, the post-collision velocities are $\boldsymbol{v}_i' = \boldsymbol{v}_i - (\hat{\boldsymbol{\sigma}}_i \cdot \boldsymbol{g}_{ij})\hat{\boldsymbol{\sigma}}_i$, $\boldsymbol{v}_j' = \boldsymbol{v}_j + (\hat{\boldsymbol{\sigma}}_i \cdot \boldsymbol{g}_{ij})\hat{\boldsymbol{\sigma}}_i$;

(v) repeat (i—iv) for another particle.

1.2 Determination of the collision modification factor

Based on the Enskog equation for dense gases[23], when a gas is so dense that the volume of all the molecules is comparable with the total volume of the system, the molecules can no longer be treated as point particles. Therefore the common position of two colliding molecules in the Boltzmann equation should be replaced by the actual positions of the centers of two tangent spheres. And the collision frequency is influenced by correlative effects that depend on the density at the point of contact.

Due to the reduced volume occupied by the molecules, a modified higher scattering probability is $\Gamma' = V/V' \cdot \Gamma_B$, where $V' = (1 - 4n\pi\sigma^3/3)$. However, the scattering probability is lowered again by another effect that the particles are screening each other. A particle might not be available for scattering with another particle because there might be a third particle in between. This effect leads to a reduction of the scattering probability by a factor of $(1 - 11n\pi\sigma^3/12)$. Including this factor, the modified scattering probability is

$$\Gamma_{HS} = \chi(n)\Gamma_B, \tag{2}$$

where $\chi(\eta) = \dfrac{1 - 11\eta/8}{1 - 2\eta}$, $\eta = \dfrac{2}{3}n\pi\sigma^3$.

This result can, however, be trusted only to the early orders in *n*, since four particle

configurations have not been considered. In the current study, the expression up to third order has been used[23]:

$$c(h) = 1 + 0.625h + 0.2869h^2 + 0.1103h^3. \tag{3}$$

It can be proved that this expression value is lower than those from the expressions of Frezzotti[22] and Kortemeyer et al.[11], while close to that from Garcia et al.[24] in their CBA introduction.

1.3 Macroscopic physical quantities

The macroscopic physical quantities of the flow field are obtained by statistic calculation as follows:

$$U_j = \frac{1}{N_j}\sum u, \tag{4}$$

where U_j is the averaged velocity in cell j, N_j is the particle number in cell j.

$$T = (3T_{\text{tr}} + z\,T_{\text{rot}})/(3 + z), \tag{5}$$

where T_{tr} is the translational temperature, T_{rot} is the rotational temperature and x is number of internal degrees of freedom. The vibrational energy is neglected. There are

$$T_{\text{tr}} = 2(\overline{mv^2} - \bar{m}\cdot\bar{v}^2)/3k, \tag{6}$$

$$T_{\text{rot}} = \frac{2}{k}(\overline{e_{\text{rot}}}/z), \tag{7}$$

where m is the molecular mass, k is the Boltzmann constant, e_{rot} is the molecular rotational energy and the overbar, $\overline{()}$ represents sample average.

The skin friction coefficient of wall surface is

$$C_{\text{f}} = \frac{t}{\frac{1}{2}r_\infty u_\infty^{\,2}} = \left\{\frac{\left[\sum(mu)_i - \sum(mu)_r\right]\cdot N_0}{\Delta t\cdot\Delta x}\right\} \Big/ \left(\frac{1}{2}r_\infty u_\infty^{\,2}\right), \tag{8}$$

where the subscript "i" and "r" represent incident and reflected molecular stream; N_0 is the number of gaseous molecules associated with a computational molecule, and Δt is the time period of sampling.

The net heat transfer flux q is the sum of the translational and rotational energies of both the incident and the reflected molecules, i.e.,

$$q = \frac{\left[\left(\sum e_{\text{tr}} + \sum e_{\text{rot}}\right)_i - \left(\sum e_{\text{tr}} + \sum e_{\text{rot}}\right)_r\right]N_0}{\Delta t\cdot\Delta x}. \tag{9}$$

2 Results and discussion

The dense gas flow in micro- and nano-channels was simulated using the ESMC method. The results were compared with those from the standard DSMC method and the CBA model. The flow and heat transfer characteristics were therefore analyzed.

Fig. 1 shows the physical model and the boundary conditions of a micro/nano gas flow. The channel is L in length and H in height. The number density of the freesteam coming gas flow is n_∞, the velocity is u_∞ and the temperature is T_∞.

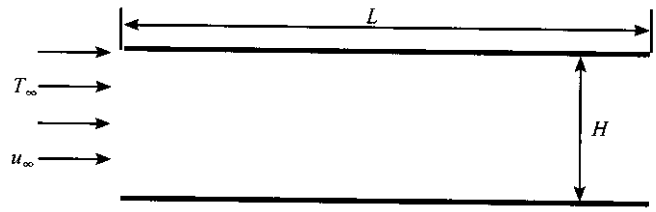

Fig. 1. Physical model and boundary conditions.

In the following calculations, L = 0.05 μm and H = 0.01 μm. The rectangular cells (100×60) and four subcells (2×2) in a cell were used. The simulation parameters of the gas N_2 are listed in Table 1, where d_{ref} and T_{ref} are reference molecular diameter and reference temperature, respectively, and w is the viscosity-temperature index. The freestream gas velocity u_∞ = 200 m/s, the temperature T_∞ = 300 K, and the wall temperature T_w = 300 K. The variable hard sphere (VHS) model was used for collisions. The completely diffuse reflection served as the gas-wall interaction. For each case, the total number of the particles exceeded 10^5, and the total sampling number was over 3×10^6.

Table 1 Parameters of N_2[10]

m/kg	z	d_{ref}/m	T_{ref}/K	w
4.65×10^{-26}	2	4.17×10^{-10}	273	0.74

Fig. 2 shows the velocity and temperature evolutions along the channel mid-line at $n_\infty = 1.29\times10^{26}$. Results of both ESMC and DSMC were plotted in the figures. The uniform coming gas flow was pressed by the boundary layer near the inlet due to the viscosity effect. Therefore the velocity was much lower than the freestream velocity. At the same time, the gas temperature became higher because of being pressed. Near the outlet, the gas expended out, the averaged velocity increased and the temperature became lower than the freestream gas temperature. In Fig. 2(a), the averaged velocity near the outlet increased, however, because the velocity profile became "full", the velocity at the mid-line appeared a little decrease.

For this case, h = 0.0196, the dense gas effect was so weak that there was little difference between the results from the ESMC and the standard DSMC methods. Fig. 2 indicated that when the gas density was not too high, ESMC would degenerate to

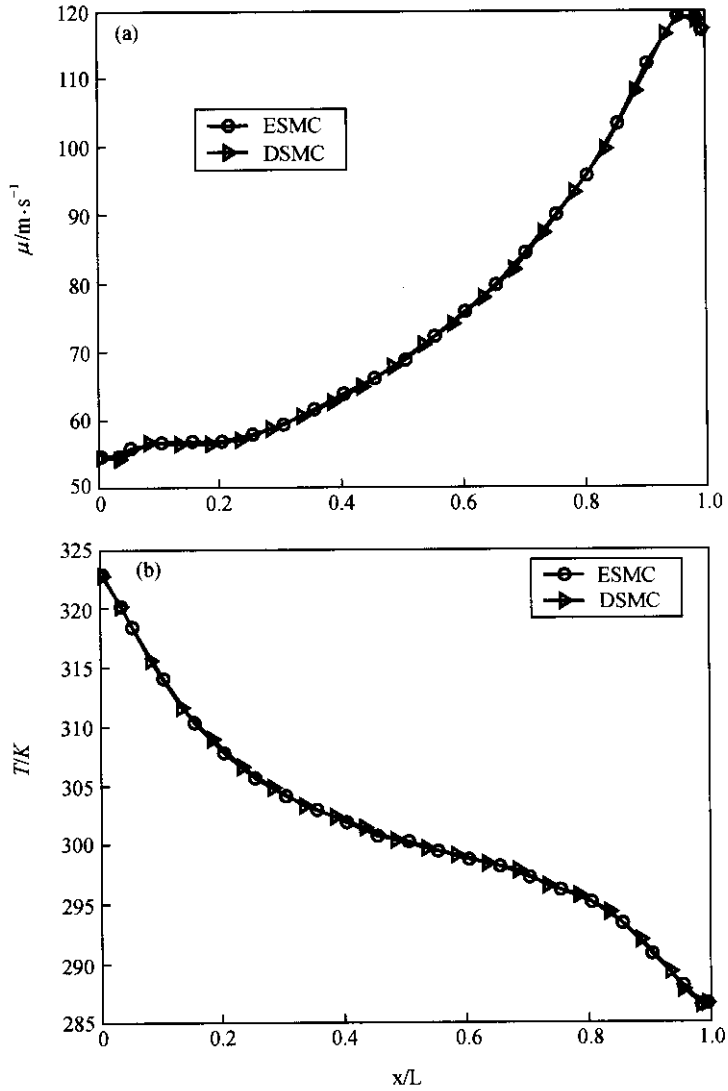

Fig. 2. Velocity and temperature evolutions along the channel mid-line at $h = 0.0196$. (a) Velocity; (b) temperature.

DSMC, which also validated the present ESMC code.

Fig. 3 shows the results at $n_\infty = 2.59\times10^{27}$. The results of CBA were also plotted in the same figure. For this case, $h = 0.393$, the dense gas effect became much stronger, so that ESMC departed from the DSMC in the velocity distribution, while agreed well with the CBA results (Fig. 3(a)). In the temperature distribution (Fig. 3(b)), there were difference between the results of two methods for dense gas flows, ESMC and CBA. The reason might lie on two aspects: i) the introduction of CBA model changed the transport coefficient of gas, and thus led to errors in macroscopic physical quantities; ii) the

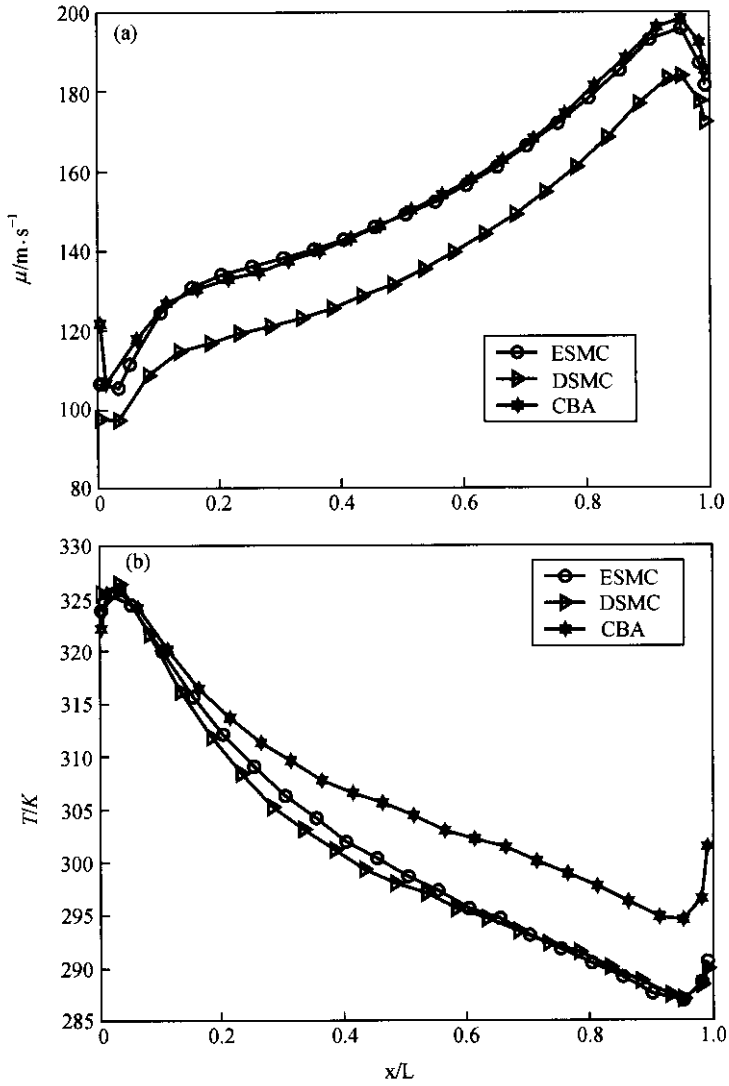

Fig. 3. Velocity and temperature evolutions along the channel mid-line at $h = 0.393$. (a) Velocity; (b) temperature.

hard sphere model used in ESMC did not embody the intermolecular force in dense gas (i.e. van der Waals force). The exact explanation needs further considerations.

Fig. 4 is the comparison of the skin friction and heat transfer characteristics on the wall surface between ESMC and DSMC at $h = 0.393$. When the dense gas effect was considered, the predicted skin friction coefficient was lower than that predicted by DSMC. The dense gas effect also changed the heat transfer characteristics on the wall surface. With the dense gas effect considered, the heat flux along the fore half channel wall was remarkably lower than DSMC results, and a little higher than DSMC results on the hind half wall.

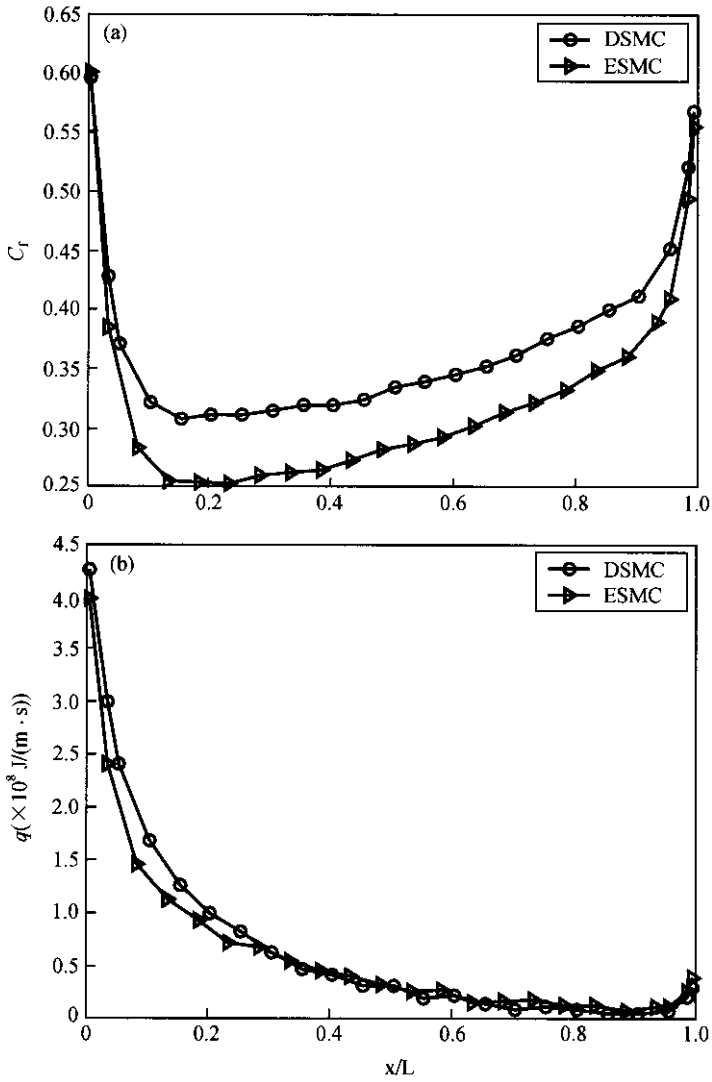

Fig. 4. Friction and heat transfer characteristics on the wall surface at h = 0.393. (a) Skin friction coefficients; (b) heat flux.

3 Concluding remarks

The Enskog simulation Monte Carlo method was applied in this paper to simulate and analyze the dense gas flow and heat transfer in micro- and nanoscale channels. The collision modification factor was determined based on the Enskog dense gas theory. The simulation results showed that when h was at small values, ESMC would degenerate to standard DSMC; when h was large enough, the dense gas effect would be remarkable: the flow field of ESMC departed from that of DSMC, while agreed well with that of CBA; however, for the temperature field, the difference between ESMC and CBA was not clear, and departed largely from CBA. The reason was in further consideration. With

the dense gas effect considered, the skin friction coefficient became lower, and the heat transfer characteristics changed also. The heat flux on the channel wall surfaces was markedly lower in the fore half and a little higher in the hind half than that in perfect gas assumption.

Acknowledgements This work was supported by the National Natural Science Foundation of China (Grant No. 59995550-2), and the National Key Basic Research and Development Program of China (Grant No. 1999033106).

References

1. Ho, C. M., Tai, Y. C., Micro-electro-mechanical-systems (MEMS) and fluid flows, Annu. Rev. Fluid Mech., 1998, 30: 579—612.
2. Guo, Z. Y., Li, Z. X., Size effect on microscale single-phase flow and heat transfer, International Journal of Heat and Mass Transfer, 2003, 46: 149—159.
3. Karniadakis, G. E., Beskok, A., Micro Flows: Fundamentals and Simulation, New York: Springer, 2002.
4. Tsien, H. S., Superaerodynamics, mechanics of rarefied gases, J. Aero. Sci., 1946, 13(12): 653—664.
5. Shen, C., Raredied Gas Dynamics (in Chinese), Beijing: National Defence Industry Publishing House, 2003.
6. Gad-el-Hak, M., The fluid mechanics of microdevices —The Freeman Scholar Lecture, J. Fluid Engin., 1999, 121: 5—33.
7. Wang, M. R., Li, Z. X., Similarity of ideal gas flow at different scales, Science in China, Ser. E, 2003, 46: 661—670.
8. Gatzen, H. H., Rigid disk slider micromachining challenges to meet microtribology needs, Tribol. Int., 2000, 33: 337—342.
9. Alexander, F. J., Garcia, A. L., Alder, B. J., A consistent Boltzmann algorithm, Physical Review Letters, 1995, 74: 5212—5215.
10. Bird, G. A., Molecular Gas Dynamics and the Direct Simulation of Gas Flows, Oxford: Clarendon Press, 1994.
11. Kortemeyer, G., Daffin, F., Bauer, W., Nuclear flow in consistent Boltzmann algorithm models, Physics Letters B, 1996, 374: 25—30.
12. Hadjiconstantinou, N. G., Garcia, A. L., Alder, B. J., The surface properties of a van der Waals fluid, Physica A, 2000, 281: 337—347.
13. Wang, M. R., Li, Z. X., Nonideal gas flow and heat transfer in micro- and nanochannels using the direct simulation Monte Carlo method, Physical Review E, 2003, 68: 046704.
14. Alexander, F. J., Garcia, A. L., Alder, B. J., The consistent Boltzmann algorithm for the van der Waals equation of state, Physica A, 1997, 240: 196—201.
15. Garcia, A. L., Alexander, F. J., Alder, B. J., A particle method with adjustable transport properties——The generalized consistent Boltzmann algorithm, J. Stat. Phys., 1997, 89: 403—409.
16. Garcia, A. L., Wagner, W., Some new properties of the kinetic equation for the consistent Boltzmann algorithm, Transport Theo. Stat., 2002, 31: 579—594.
17. Kauzmann, W., Kinetic Theory of Gases, New York: Benjamin, Inc., 1976.
18. Dufty, J. W., Santos, A., Brey, J. J., Practical kinetic model for hard sphere dynamics, Physical Review Letter, 1996, 77: 1270—1273.
19. Wagner, W., A convergence proof for Bird's direct simulation Monte Carlo method for the Boltzmann equation, J. Stat. Phys., 1992, 66: 1011—1044.
20. Montanero, J. M., Santos, A., Monte Carlo simulation method for the Enskog equation, Physical Review E, 1996, 54: 438—444.
21. Montanero, J. M., Santos, A., Simulation of Enskog Equation a la Bird, Phys. Fluids., 1997, 9(7): 2057—2060.
22. Frezzotti, A., Particle scheme for the numerical solution of the Enskog equation, Phys. Fluids., 1997, 9(5): 1329—1335.
23. Schram, P. P., Kinetic, J. M., Theory of Gas and Plasmas, Dordrecht: Kluwer Academic Pulishers, 1991.
24. Garcia, A., Baras, F., Direct simulation Monte Carlo: Novel application and new extensions, in Proceedings of the 3rd Workshop on Modelling of Chemical Reaction Systems, Heidelberg, 1997.